

COMPLEX WAVELET JOINT DENOISING AND DEMOSAICING USING GAUSSIAN SCALE MIXTURES

Bart Goossens, Jan Aelterman, Hiêp Luong, Aleksandra Pižurica and Wilfried Philips

Ghent University - TELIN - IPI - iMinds
Sint-Pietersnieuwstraat 41, B-9000 Ghent, Belgium
bart.goossens@telin.ugent.be

ABSTRACT

Wavelet-based demosaicing techniques have the advantage of being computationally relatively fast, while having a reconstruction performance that is similar to state-of-the-art techniques. Because the demosaicing rules are linear, it is fairly simple to integrate denoising into the demosaicing. In this paper, we present a method that performs joint denoising and demosaicing, using a Gaussian Scale Mixture (GSM) prior model, thereby modeling the local edge direction as a hidden variable. The results indicate that this technique offers a better reconstruction performance (in PSNR sense and visually) than sequential demosaicing and denoising. On a recent GPU, our algorithm takes 3.5 s for reconstructing a 12 megapixel RAW digital camera image.

Index Terms—Demosaicing, Image denoising, Bayer Pattern, Complex wavelets

I. INTRODUCTION

The use of color filter arrays (CFAs), such as the Bayer CFA is still very popular due to price and power consumption reasons. While in the past, demosaicing and denoising has mostly been performed sequentially, recently some researchers [1]–[4] have explored *joint* demosaicing and denoising (sometimes called *denoising* [3]). Joint processing has the advantage that a number of problems of the sequential approach (e.g., artifacts due to incorrect selection of the interpolation direction and removal of high frequencies) can now be solved.

While some techniques perform the demosaicing entirely in the image domain (e.g., [1], [3]), it is beneficial to apply the demosaicing in the wavelet domain of the CFA mosaic image. The CFA mosaic image is a superposition of the individual CFA component images and contains both chrominance and luminance information, either non-modulated (chrominance and luminance) or modulated (chrominance). As shown by Hirakawa in [5], simple linear demosaicing rules can be derived to de-modulate or de-multiplex the chrominance and luminance information in the wavelet domain. Despite being very elegant and straightforward, one limitation are the hard assumptions required for the chrominance and luminance bandwidths. These assumptions are often violated in practice, resulting in color and zipper artifacts. In recent work, we extended the approach of Hirakawa to the complex wavelet domain and by integrating local spatial adaptivity in the algorithm, it becomes possible to alleviate the problems with the

B. Goossens is a postdoctoral researcher of the Fund for the Scientific Research in Flanders (FWO) Belgium.

bandwidth assumptions [6]. Moreover, we were also able to recover some of the high frequency luminance information.

In general, wavelet-based demosaicing algorithms tend to reconstruct high-frequencies in a natural-looking way, and the algorithms have a relatively low computational time. Because the demosaicing rules are linear, it is fairly simple to integrate denoising into the demosaicing, within the same statistical framework [2], [7]. Whereas [2], [7] mainly focus on soft-thresholding and Wiener filtering for noise removal, in this work, we consider Bayesian Least Squares estimation under a Gaussian Scale Mixture (GSM) prior model. The GSM prior model (see Portilla et al. [8]) is one of the state-of-the-art image priors for the wavelet domain. We consider several refinements in our modeling: as in [6], [9], we take the local edge direction into account. In a statistical framework, this is done by modeling the unknown edge direction as a *hidden variable*. Next, the dual-tree complex wavelet packet transform (DT-CWPT) from [10] performs a directional analysis in 6 directions (opposed to the 3 directions of the discrete wavelet transform). To obtain this directional analysis, a “complex phase modulation” (PM) step is performed [10]. Because the PM hampers the demosaicing reconstruction but is necessary for the directional selectivity, we treat this step in a special way, by including it in the demosaicing formulas.

The core idea of our approach is then 1) to exploit the properties of the DT-CWPT for modeling edges in reconstructed images, 2) to perform demosaicing in DT-CWPT transform domain in a spatially-adaptive way and 3) to integrate this approach in a vector-based wavelet denoiser (here: BLS-GSM). This leads to a joint denoising and demosaicing approach, in which several problems are tackled in a clever way.

The remainder of this paper is structured as follows: in Section II, we discuss the image and noise modeling that is used in this paper. Section III describes the proposed joint denoising and demosaicing approach. In Section IV, experimental results are given and discussed. Section V concludes this paper.

II. IMAGE AND NOISE MODELING

Consider an RGB color image, consisting of a red $R(\mathbf{p})$, green $G(\mathbf{p})$ and blue channel $B(\mathbf{p})$, with $\mathbf{p} = [p_1, p_2]$ the discrete spatial position. For the Bayer CFA, the red, green and blue channels will be sub-sampled according to the following operation:

$$\begin{aligned} R_m(\mathbf{p}) &= R(\mathbf{p}) (1 + (-1)^{p_1} - (-1)^{p_2} - (-1)^{p_1+p_2}) / 4 \\ G_m(\mathbf{p}) &= G(\mathbf{p}) (1 + (-1)^{p_1+p_2}) / 2 \\ B_m(\mathbf{p}) &= B(\mathbf{p}) (1 - (-1)^{p_1} + (-1)^{p_2} - (-1)^{p_1+p_2}) / 4 \end{aligned} \quad (1)$$

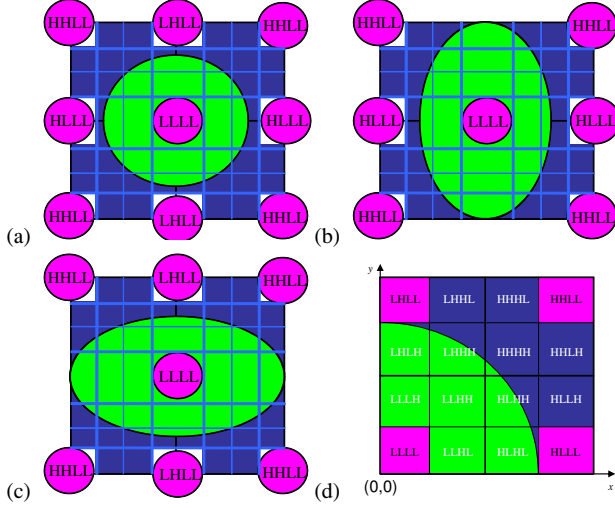


Fig. 1. Frequency domain tiling of the DT-CWPT demosaicing scheme. Green is luminance, magenta represents chrominance. (a) Default bandwidth assumptions ($q = 1/2$), (b) Modified assumptions for horizontal edge ($q = 1$), (c) Modified assumptions for vertical edge ($q = 0$). (d) DT-CWPT Subband names.

Similar sub-sampling formulas can be written for other (non-Bayer) CFA designs. In each case, the CFA mosaic image is simply the sum of the three sub-sampled signals:

$$M(\mathbf{p}) = R_m(\mathbf{p}) + G_m(\mathbf{p}) + B_m(\mathbf{p}). \quad (2)$$

Employing a Poissonian-Gaussian approximation of signal-dependent noise [11], [12], we assume the following signal+noise model for the measured CFA mosaic image:

$$M(\mathbf{p}) = X(\mathbf{p}) + \sigma_{\mathbf{p}}^2(X(\mathbf{p}))W(\mathbf{p}), \quad (3)$$

where $X(\mathbf{p})$ is the “ideal” noise-free CFA mosaic image, and where $W(\mathbf{p})$ is white Gaussian noise $N(0, 1)$. Here, $\sigma_{\mathbf{p}}^2(X(\mathbf{p}))$ is a channel and signal-dependent noise variance. For the purpose of this paper, we will consider stationary noise with constant variance $\sigma_{\mathbf{p}}^2(X(\mathbf{p})) = \sigma_0^2$, keeping in mind that our approach can easily be extended to the more general case (using techniques from [7], [12]–[14]).

III. JOINT DENOISING AND DEMOSAICING

A schematic overview of our approach is depicted in Figure 2. First, we apply the two-scale 2D DT-CWPT [15] transform to the CFA mosaic image $M(\mathbf{p})$. In contrast to [15], the phase modulation (PM) to compute the complex-valued coefficients is not applied at this stage (this will be done later in this section). Doing so, we obtain 4 times 16 *real-valued* wavelet packet subbands. Let $M_{klmn}^{(i)}$ (with $k, l, m, n = H, L$) denote a wavelet coefficient at position \mathbf{p} of the $klmn$ -subband (see Figure 1(d)) of DT-CWPT tree $i = 1, \dots, 4$ (see Figure 2). To simplify the notations, we will consider one fixed position the same time so that we can drop \mathbf{p} in the following. Furthermore, let us denote by $R_{klmn}^{(i)}$, $G_{klmn}^{(i)}$, $B_{klmn}^{(i)}$ the DT-CWPT of respectively $R(\mathbf{p})$, $G(\mathbf{p})$ and $B(\mathbf{p})$. The demosaicing rules of our approach from [9] (which does not include denoising) are summarized in Table I. In Table I, the position-dependent variable q represents the estimated edge direction at the

Table I. Locally adaptive complex wavelet demosaicing rules [9].

<p>1) Luminance information (non-LHLL/HLLL/LLLL subbands): $R_{klmn} = G_{klmn} = B_{klmn} = Y_{klmn} = M_{klmn}$ where $mn = LH, HL, HH, k = H, L, l = H, L$ $R_{HHLL} = G_{HHLL} = B_{HHLL} = Y_{klmn} = 0$</p> <p>2) Directionally adaptive reconstr. of high frequency luminance information (LHLL and HLLL subbands): $R_{LHLL} = G_{LHLL} = B_{LHLL} = q \left(s_{LHLL}^G M_{LHLL} - s_{HLLL}^G M_{HLLL} \right)$ $R_{HLLL} = G_{HLLL} = B_{HLLL} = (q-1) \left(s_{LHLL}^G M_{LHLL} - s_{HLLL}^G M_{HLLL} \right)$</p> <p>3) Combined luminance and chrominance (LLLL subband): $G_{LLLL} = M_{LLLL} - s_{HHLL} M_{HHLL}$ $R_{LLLL} = 2(s_{HHLL} M_{HHLL} + (1-q) s_{LHLL}^R M_{LHLL} + q s_{HLLL}^R M_{HLLL}) + M_{LLLL}$ $B_{LLLL} = 2(s_{HHLL} M_{HHLL} + (1-q) s_{LHLL}^B M_{LHLL} + q s_{HLLL}^B M_{HLLL}) + M_{LLLL}$</p>
--

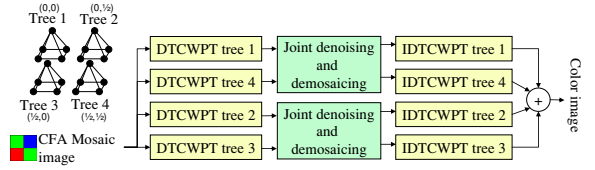


Fig. 2. Overview of the joint denoising and demosaicing scheme.

considered position \mathbf{p} . It is defined as follows:

$$q = \begin{cases} 0 & \text{vertical edge} \\ 0.5 & \text{unsure} \\ 1 & \text{horizontal edge} \end{cases} \quad (4)$$

Next, the variables $s_{LHLL}^R, s_{LHLL}^G, s_{LHLL}^B, s_{HLLL}^R, s_{HLLL}^G, s_{HLLL}^B, s_{HHLL}$ are -1 or 1 , depending on the shifts of p_1 and p_2 used in (1) (see [9]). For example, for the Bayer pattern from Figure 2, we have $s_{HHLL} = s_{HLLL}^R = s_{LHLL}^G = s_{LHLL}^B = -1$ and $s_{LHLL}^R = s_{LHLL}^G = s_{HLLL}^B = 1$.

After applying the demosaicing rules, we want to benefit from the improved directional selectivity obtained by the PM, we will take this operation into account for the *denoising* part of our algorithm. In particular, the PM is performed as follows [15]:

$$\begin{pmatrix} M_{klmn}^{(r1)} \\ M_{klmn}^{(i1)} \end{pmatrix} = \mathbf{P} \begin{pmatrix} M_{klmn}^{(1)} \\ M_{klmn}^{(4)} \end{pmatrix}, \quad \begin{pmatrix} M_{klmn}^{(r2)} \\ M_{klmn}^{(i2)} \end{pmatrix} = \mathbf{P} \begin{pmatrix} M_{klmn}^{(2)} \\ M_{klmn}^{(3)} \end{pmatrix} \quad (5)$$

where $\mathbf{P} = \frac{1}{\sqrt{2}} \begin{pmatrix} 1 & 1 \\ -1 & 1 \end{pmatrix}$. $M_{klmn}^{(r1)} + jM_{klmn}^{(i1)}$ and $M_{klmn}^{(r2)} + jM_{klmn}^{(i2)}$ are then the resulting complex wavelet coefficients (here j is the imaginary unit).

In the remainder of this Section, we consider the three types of demosaicing rules from Table I. We express these rules each time in the Bayesian framework, to obtain estimators that jointly perform denoising and demosaicing.

III-A. Highpass luminance information

According to step 1) in Table I, the highpass luminance components can directly be obtained from the DT-CWPT of the mosaic image ($R_{klmn} = G_{klmn} = B_{klmn} = M_{klmn}$). Now we will extend this step to include denoising, through (5). The Bayesian least

squares estimator is given by:

$$\begin{aligned}\hat{\mathbf{X}}_{klmn} &= \mathbb{E}[\mathbf{X}_{klmn}|\mathbf{M}_{klmn}], \\ &= \mathbb{E}_{z, \mathbf{M}_{klmn}}[\mathbb{E}[\mathbf{X}_{klmn}|\mathbf{M}_{klmn}, z]]\end{aligned}\quad (6)$$

where \mathbf{M}_{klmn} and \mathbf{X}_{klmn} are vectors formed by column-stacking the local 3×3 neighborhood around \mathbf{p} of respectively $M_{klmn}^{(r1)}$ and $X_{klmn}^{(r1)}$ (after PM). z is the hidden multiplier of the GSM model [8]. Analogous equations hold for $M_{klmn}^{(i1)}$, $M_{klmn}^{(r2)}$, $M_{klmn}^{(i2)}$ and $X_{klmn}^{(i1)}$, $X_{klmn}^{(r2)}$, $X_{klmn}^{(i2)}$. When modeling \mathbf{X}_{klmn} using a Gaussian Scale Mixture, $\mathbb{E}_{z, \mathbf{M}_{klmn}}[\mathbb{E}[\mathbf{X}_{klmn}|\mathbf{M}_{klmn}, z]]$ is precisely the BLS-GSM estimator derived in [8].

III-B. Directionally adaptive estimation of the LHLL and HLLL subbands

To extend step 2) in Table I, we model the edge direction q using a *hidden* variable. Let $\mathbf{Y}_{klmn} = (Y_{LHLL}^{(1)} Y_{HLLL}^{(1)} Y_{LHLL}^{(4)} Y_{HLLL}^{(4)})^T$ be a vector with wavelet coefficients of the luminance data to be estimated and let $\mathbf{M}_{klmn} = (M_{LHLL}^{(r1)} M_{HLLL}^{(i1)})^T$ be wavelet coefficients of the observed CFA image. Then, the equations in Table I can be written in matrix-form, as follows:

$$\begin{aligned}\mathbf{Y}_{klmn} &= (\mathbf{P} \otimes \mathbf{A}(q)) \mathbf{M}_{klmn} \\ &= (\mathbf{P} \otimes \mathbf{A}(q)) \mathbf{X}_{klmn} + (\mathbf{P} \otimes \mathbf{A}(q)) \mathbf{W}_{klmn}, \quad \text{with} \\ \mathbf{A}(q) &= \begin{pmatrix} q s_{LHLL}^G & -q s_{HLLL}^G \\ -(1-q) s_{LHLL}^G & (1-q) s_{HLLL}^G \end{pmatrix}\end{aligned}$$

where ' \otimes ' is the Kronecker product. For the assumed signal+noise model (3), this gives:

$$\mathbf{Y}_{klmn} = \underbrace{(\mathbf{P} \otimes \mathbf{A}(q)) \mathbf{X}_{klmn}}_{\tilde{\mathbf{x}}_{klmn} \text{ (signal)}} + \underbrace{\sigma_0^2 (\mathbf{P} \otimes \mathbf{A}(q)) \mathbf{W}_{klmn}}_{\text{(noise)}}$$

Now, we wish to reconstruct the signal $\tilde{\mathbf{x}}_{klmn}$, the PM'ed and demosaiced version of \mathbf{X}_{klmn} . The BLS estimate is given by:

$$\begin{aligned}\hat{\tilde{\mathbf{x}}}_{klmn} &= \mathbb{E}[\tilde{\mathbf{x}}_{klmn}|\mathbf{Y}_{klmn}], \\ &= \mathbb{E}_{q|\mathbf{Y}_{klmn}}[\mathbb{E}[\tilde{\mathbf{x}}_{klmn}|\mathbf{Y}_{klmn}, q]] \\ &= \mathbb{E}_{q|\mathbf{Y}_{klmn}}[\mathbb{E}_{z|q, \mathbf{Y}_{klmn}}[\mathbb{E}[\tilde{\mathbf{x}}_{klmn}|\mathbf{Y}_{klmn}, z, q]]].\end{aligned}$$

Again, $\mathbb{E}_{z|q, \mathbf{Y}_{klmn}}[\mathbb{E}[\tilde{\mathbf{x}}_{klmn}|\mathbf{Y}_{klmn}, z, q]]$ is the BLS-GSM estimator (but here conditioned on q). Practically, three BLS-GSM estimates are evaluated according to $q = 0, 1/2, 1$, and subsequently a weighted mean is calculated based on the weights $p(q|\mathbf{Y}_{klmn})$ (the posterior probability that a given edge direction q is observed, given the observed vector \mathbf{Y}_{klmn}). The weights $p(q|\mathbf{Y}_{klmn})$ can further be calculated as outlined in [9]. The main idea is to characterize $\mathbf{Y}_{LHLL}|q=0$ by having a large L_1 norm (assuming that a vertical edge causes wavelet coefficients with a large magnitude in the LHLL band), while correspondingly $\mathbf{Y}_{HLLL}|q=0$ will cause a *small* L_1 norm (and vice versa for $\mathbf{Y}_{LHLL}|q=1$ and $\mathbf{Y}_{HLLL}|q=1$). In the absence of edges ($q = 1/2$), we should have $\mathbf{Y}_{LHLL} = \mathbf{Y}_{HLLL}$. We therefore choose:

$$\begin{aligned}b_{\min} &= \min(\|\mathbf{Y}_{HLLL}\|, \|\mathbf{Y}_{LHLL}\|) \quad \text{and} \\ b_{\max} &= \max(\|\mathbf{Y}_{HLLL}\|, \|\mathbf{Y}_{LHLL}\|), \quad \text{then:}\end{aligned}$$

Table II. Locally adaptive complex wavelet *joint* denoising and demosaicing rules.

<p>1) Luminance information (non-LHLL/HLLL/LLLL subbands): $\hat{\mathbf{R}}_{klmn} = \hat{\mathbf{G}}_{klmn} = \hat{\mathbf{B}}_{klmn} = \hat{\mathbf{X}}_{klmn} = \mathbb{E}[\mathbf{X}_{klmn} \mathbf{M}_{klmn}]$, where $mn = LH, HL, HH$, $k = H, L$, $l = H, L$ $\hat{\mathbf{R}}_{HHLL} = \hat{\mathbf{G}}_{HHLL} = \hat{\mathbf{B}}_{HHLL} = 0$</p> <p>2) Directionally adaptive reconstr. of high frequency luminance information (LHLL and HLLL subbands): $\hat{\tilde{\mathbf{x}}}_{klmn} = \mathbb{E}_{q \mathbf{Y}_{klmn}}[\mathbb{E}_{z q, \mathbf{Y}_{klmn}}[\mathbb{E}[\tilde{\mathbf{x}}_{klmn} \mathbf{Y}_{klmn}, z, q]]]$ where $\mathbf{Y}_{klmn} = \begin{pmatrix} q s_{LHLL}^G & -q s_{HLLL}^G \\ -(1-q) s_{LHLL}^G & (1-q) s_{HLLL}^G \end{pmatrix} \mathbf{M}_{klmn}$</p> <p>3) Combined luminance and chrominance (LLLL subband): $\hat{\tilde{\mathbf{x}}}_{LLLL} = \mathbb{E}_{q \mathbf{Y}_{LLLL}}[\mathbb{E}_{z q, \mathbf{Y}_{LLLL}}[\mathbb{E}[\tilde{\mathbf{x}}_{LLLL} \mathbf{Y}_{LLLL}, z, q]]]$ where $\mathbf{Y}_{LLLL} = \begin{pmatrix} 1 & 0 & 0 & -s_{HLLL} \\ 1 & 2(1-q)s_{LHLL,r} & 2q s_{HLLL,r} & 2s_{HLLL}^R \\ 1 & 2(1-q)s_{LHLL,b} & 2q s_{HLLL,b} & 2s_{HLLL,b} \end{pmatrix} \mathbf{M}_{LLLL}$</p>

$$q = \begin{cases} 1/2 & \frac{\|\mathbf{Y}_{HLLL}\|}{b_{\max}} < \log \frac{14}{5} - \frac{\|\mathbf{Y}_{LHLL}\|}{b_{\min}} \quad \text{and} \\ & \frac{\|\mathbf{Y}_{HLLL}\|}{b_{\max}} < \log \frac{14}{5} - \frac{\|\mathbf{Y}_{LHLL}\|}{b_{\min}} \\ 1 & \|\mathbf{Y}_{LHLL}\| < \|\mathbf{Y}_{HLLL}\| \\ 0 & \text{else} \end{cases}$$

where the constant $\frac{14}{5}$ is chosen to minimize the reconstruction error (see [9]). Based on these findings, the probabilities $p(q|\mathbf{Y}_{klmn})$ can directly be calculated (the details are omitted here because of space limitations). Finally, the procedure is repeated for third and fourth trees (i.e., for $\mathbf{Y}_{klmn} = (Y_{LHLL}^{(3)} Y_{HLLL}^{(3)} Y_{LHLL}^{(4)} Y_{HLLL}^{(4)})^T$ and $\mathbf{M}_{klmn} = (M_{LHLL}^{(r2)} M_{HLLL}^{(i2)})^T$.

III-C. Estimation of the LLLL-subband

Let $\mathbf{Y}_{klmn} = (G_{LLLL}^{(r1)} R_{LLLL}^{(r1)} B_{LLLL}^{(r1)} G_{LLLL}^{(i1)} R_{LLLL}^{(i1)} B_{LLLL}^{(i1)})^T$ and let $\mathbf{M}_{klmn} = (M_{LLLL}^{(1)} M_{HLLL}^{(1)} M_{LHLL}^{(1)} M_{HLLL}^{(1)} M_{LLLL}^{(4)} M_{HLLL}^{(4)} M_{LHLL}^{(4)} M_{HLLL}^{(4)})^T$, then according to Table I and (5) we find:

$$\begin{aligned}\mathbf{Y}_{klmn} &= (\mathbf{P} \otimes \mathbf{A}'(q)) \mathbf{M}_{klmn} \quad \text{with} \\ \mathbf{A}'(q) &= \begin{pmatrix} 1 & 0 & 0 & -s_{HLLL} \\ 1 & 2(1-q)s_{LHLL,r} & 2q s_{HLLL,r} & 2s_{HLLL}^R \\ 1 & 2(1-q)s_{LHLL,b} & 2q s_{HLLL,b} & 2s_{HLLL,b} \end{pmatrix}\end{aligned}\quad (7)$$

The estimation procedure is then entirely analogous to Subsection III-B, the only difference is that the grouping of the wavelet coefficients into vectors is different, as well as the transform matrix (in this case $\mathbf{A}'(q)$). As in Subsection III-B, the same procedure is then also repeated for the third and fourth tree.

IV. RESULTS AND DISCUSSION

To validate the performance of the proposed method, we corrupted the kodim04 image of the Kodak image database with white Gaussian noise with standard deviation $\sigma = 10$. We subsampled the image according to Bayer pattern from Figure 2, and we reconstructed the image using both the complex wavelet demosaicing (without denoising) and the proposed approach (with denoising). The results are shown in Figure 3, where we compare to the sequential approaches denoising-post-demosaicing and demosaicing-post-denoising. Even though the proposed approach is

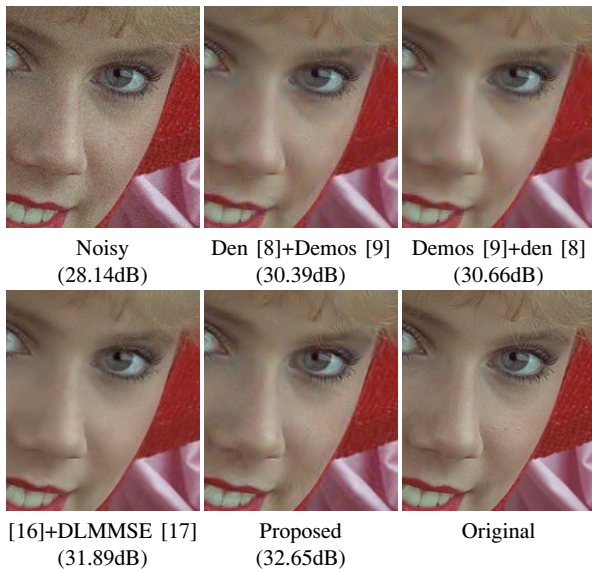


Fig. 3. Joint denoising and demosaicing (artificially added noise $\sigma = 10$).

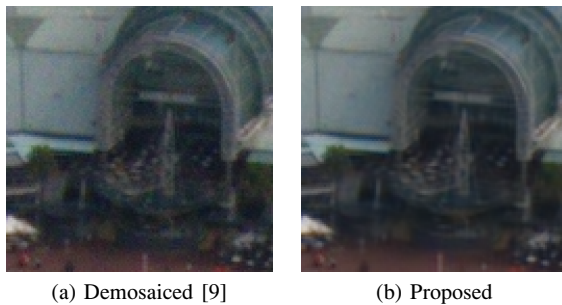


Fig. 4. Results for RAW digital camera data.

a joint demosaicing and denoising method, the noise is removed well, while many image details (e.g., the eyelashes) are slightly sharper than in [16]+DLMMSE [17].

Finally, we also integrated the proposed method in a digital camera reconstruction algorithm for RAW images, that works on a GPU using CUDA. A RAW digital camera image (of Darling Harbour in Sydney) was captured using a Panasonic DMC-FZ38, with ISO: 80, shutter speed 1/250s and resolution 3016×4016 (12 megapixels). Cropped versions of the results are shown in Figure 4. Here, the proposed method suppresses the noise well, while preserving edges and other fine structures. The complete reconstruction of the 12 megapixel image took 3.5 s (NVIDIA GeForce GTX 560Ti).

V. CONCLUSION

In this paper, we have presented a new joint demosaicing and denoising scheme that is tailored to the complex wavelet packet transform and that fully exploits the properties of the complex wavelets (e.g., approximate shift-invariance, directional selectivity). The scheme is based on a Bayesian Least Squares estimate for a GSM prior, involving two hidden variables: the hidden GSM

multiplier, as well as the local edge direction. Experimental results demonstrate that the proposed approach is well suited to remove noise during demosaicing, while image details are being preserved. The proposed scheme is especially promising because of its low computational requirements (especially on a recent GPU), so that very large images can be reconstructed in less than 4 seconds. To simplify the analysis, stationary noise was assumed in this paper. Nevertheless, the noise model can easily be extended to signal-dependent noise (e.g., to better deal with low-light scenarios), using modeling techniques such as the one proposed in [11], [18]. This will be a topic of our future work.

VI. REFERENCES

- [1] K. Hirakawa and T. W. Parks, "Joint demosaicing and denoising," *IEEE Trans. Image Process.*, vol. 15, pp. 2146–2157, aug 2006.
- [2] K. Hirakawa, *Single-Sensor Imaging: Methods and Applications for Digital Cameras*, ch. Color Filter Array Image Analysis for Joint Denoising and Demosaicking. CRC Press, 2008.
- [3] L. Condat, "A simple, fast and efficient approach to denoising: Joint demosaicing and denoising," in *Proc. 17th IEEE Int Conf. Image Processing (ICIP)*, (Hong Kong, China), pp. 905–908, 2010.
- [4] P. Chatterjee, N. Joshi, K. S. B., and Y. Matsushita, "Noise suppression in low-light images through joint denoising and demosaicing," in *Proc. IEEE Conf. Computer Vision and Pattern Recognition (CVPR)*, pp. 321–328, 2011.
- [5] K. Hirakawa, X.-L. Meng, and P. J. Wolfe, "A framework for wavelet-based analysis and processing of color filter array images with applications to denoising and demosaicing," *IEEE Int. Conf. Acoust. Speech Signal Process. (ICASSP 2007)*, pp. 597–600, Apr. 2007.
- [6] J. Aelterman, B. Goossens, H. Luong, A. Pizurica, and W. Philips, "Locally Adaptive Complex Wavelet-Based Demosaicing for Color Filter Array Images," in *SPIE Electronic Imaging 2009*, (San José, CA, USA), pp. 72480J–1–12, jan 2009.
- [7] K. Hirakawa, "Signal-dependent noise characterization in Haar filterbank representation," in *Proc. SPIE Optics & Photonics*, pp. 67011I.1–67011I.12, 2007.
- [8] J. Portilla, V. Strela, M. Wainwright, and E. Simoncelli, "Image denoising using scale mixtures of gaussians in the wavelet domain," *IEEE Trans. on image processing*, vol. 12, pp. 1338–1351, Nov. 2003.
- [9] J. Aelterman, B. Goossens, A. Pizurica, and W. Philips, "Fast, locally adaptive demosaicing of color filter array images using the dual-tree complex wavelet packet transform." Submitted to PLoS ONE, 2013.
- [10] I. W. Selesnick, R. G. Baraniuk, and N. G. Kingsbury, "The Dual-Tree Complex Wavelet Transform," *IEEE Signal Processing Magazine*, vol. 22, pp. 123–151, nov 2005.
- [11] A. Foi, M. Trimeche, V. Katkovnik, and K. Egiazarian, "Practical poissonian-gaussian noise modeling and fitting for single-image raw-data," *IEEE Trans. image Process.*, vol. 17, pp. 1737–1754, Oct. 2008.
- [12] B. Goossens, A. Pizurica, and W. Philips, "Wavelet domain image denoising for non-stationary and signal-dependent noise," in *IEEE International Conference on Image Processing (ICIP)*, (Atlanta, GA, USA), pp. 1425–1428, oct 2006.
- [13] J. Portilla, "Image restoration using Gaussian Scale Mixtures in Overcomplete Oriented Pyramids (a review)," in *Proc. of the SPIE's 50th Annual Meeting: Wavelets XI*, vol. 5914, (San Diego, CA), pp. 468–482, aug 2005.
- [14] A. Foi, R. Bilcu, V. Katkovnik, and K. Egiazarian, "Adaptive-size block transforms for signal-dependent noise removal," in *Proc. 7th Nordic Sig. Proc. Symposium NORSIG 2006*, pp. 94–97, 2006.
- [15] I. W. Selesnick, R. G. Baraniuk, and N. G. Kingsbury, "The Dual-Tree Complex Wavelet Transform," *IEEE Signal Processing Magazine*, vol. 22, pp. 123–151, nov 2005.
- [16] L. Zhang, R. Lukac, X. Wu, and D. Zhang, "PCA-based Spatially Adaptive Denoising of CFA Images for Single-Sensor Digital Cameras," *IEEE Trans. Image Processing*, vol. 18, no. 4, pp. 797–812, 2009.
- [17] L. Zhang and X. Wu, "Color demosaicking via directional linear minimum mean square-error estimation," *IEEE Transactions on Image Processing*, vol. 14, pp. 2167–2178, December 2005.
- [18] B. Goossens, H. Luong, J. Aelterman, A. Pizurica, and W. Philips, "Realistic Camera Noise Modeling with Application to Improved HDR Synthesis," *EURASIP Journal on Advances in Signal Processing*, vol. 171, pp. 1–28, 2012.